ELSEVIER

Earth and Planetary Science Letters 158 (1998) 19–29

EPSL

Rheological transitions and the progress of melting of crustal rocks

Scott A. Barboza *, George W. Bergantz

Department of Geological Sciences, University of Washington, Seattle, WA 98195, USA

Received 17 April 1997; revised version received 3 December 1997; accepted 13 January 1998

Abstract

High-grade igneous and metamorphic systems which possess a variable percentage of melt, may undergo a transition between crystal-supported and fully fluid behavior. The melt-fraction interval over which this transition occurs is not well constrained. We have conducted six series of numerical simulations of crustal melting using melt-fraction intervals between 0.05 to 0.15 for this mechanical transition. The results of these simulations demonstrate the dependence of convection and progress of melting on the rheological transition between solid and melt. Convective heat flux varied by a factor of 8 over the duration of the simulations (160 yr) and the mass of melt produced varied by nearly a factor of 4. The onset of convection in simulations with the most gradual rheological transition was suppressed. Convective heat flux and progress of melting were more sensitive to the melt-fraction interval for the rheological transition than to the composition of a range of crustal protoliths. The rheological transition between solid and melt may be one of the dominant factors controlling the thermal evolution of high-grade crustal rocks.

Keywords: anatexis; mixing; melts; phase equilibria; rheology; underplating

1. Introduction

The rheological transition between solid and melt may strongly influence the thermal evolution of high-temperature igneous and metamorphic systems. Changes in the viscosity and density, as a function of the local melt fraction, contribute to the efficiency of convective heat transfer. Quantitative thermophysical models for such systems require constitutive equations which include the variability in rheological properties over the full range of melt fraction. Two end-member rheological states can be recognized in natural systems: (1) fully fluid behavior; and (2) a nearly rigid solid with a crystal-supported pore structure. The transition between these end-members need not be abrupt, but will vary as a function of the system properties and the strain rate. In this study, we demonstrate that the choice of the melt-fraction interval for the rheological transition can significantly influence the predicted thermal evolution of crystal–melt mixtures during melting or solidification.

One model for the rheological transition from crystal-supported to fully fluid behavior is an abrupt transition over a small melt-fraction interval. The melt fraction at which this transition takes place has been termed the rheological critical melt percentage [1], or critical melt fraction (CMF) [2]. The CMF model assumes that a large change in rock strength occurs over a small melt-fraction interval that falls between 28 and 50% melt. This model was inferred from the results of low-melt-fraction deformation studies in which this transition may have been observed [1,2]. The CMF model is also

* Corresponding author. Tel.: +1 (206) 543-1975; Fax: +1 (206) 543-3836; E-mail: barboza@u.washington.edu

0012-821X/98/$19.00
PII S0012-821X(98)00047-8

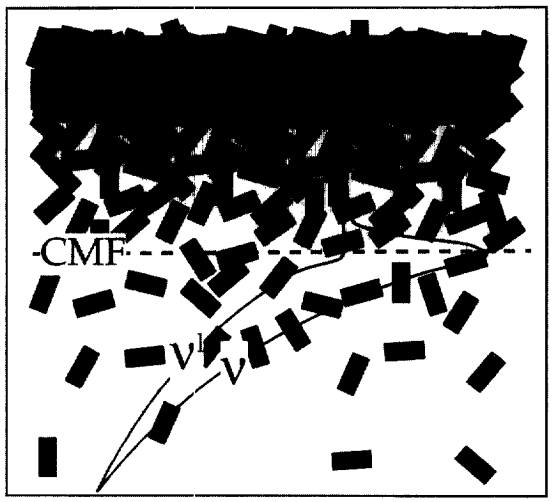

Fig. 1. Schematic depiction of the CMF model. When the local melt fraction (f') is less than the CMF, the melt percolates through a rigid solid matrix. When the CMF is exceeded, the solids are suspended in the melt and increase the effective kinematic viscosity of the mixture (ν) relative to the crystal-free melt (ν').

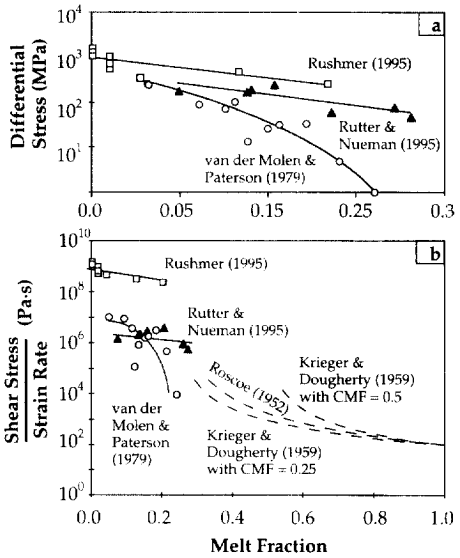

Fig. 2. Summary of experimental results related to the CMF. (a) The maximum differential stress prior to sample failure attained in three low-melt fraction deformation experiments. A large decrease in rock strength as a function of melt fraction was observed in the experiments of van der Molen and Paterson [2], leading to the inference of the CMF. This change in rheological behavior was not observed in the experiments of Rutter and Neuman [7] and Rushmer [6]. (b) The effective viscosity (shear stress/strain rate) of several experiments. This figure also depicts empirical and theoretical relationships for the viscosity of viscous suspensions [2,40].

in agreement with theoretical calculations and the results of experiments with dilute suspensions [3–5]. Fig. 1 schematically depicts the CMF model for the transition from a crystal-supported system to a suspension with the concomitant increase in the viscosity of the mixture. Empirical relationships for the viscosity of suspensions and data from relevant deformation experiments are illustrated in Fig. 2.

However, the results of several low-melt-fraction deformation experiments (Fig. 2) are not in accordance with those of the earlier studies [6,7]. These experimental results indicate that there may be a melt-fraction interval over which local variations in melt fraction, composition, microscopic pore geometry, and strain rate dictate local variations in the rheological response of the mixture. In addition, Vigneresse et al. [8] and Wildemuth and Williams [5], based on experimental results and field observations, suggested that the rheological transition may proceed through two or more stages rather than occur at a single melt fraction. Sawyer [9] observed that the experimental work supporting the CMF model was conducted in the brittle deformation regime. The majority of crustal melts are generated in the plastic deformation regime which may obscure an abrupt rheological transition. These experiments and observations document the uncertainty in the applicability of the CMF model for a wide range of geological conditions.

This uncertainty may be significant, because the general validity of the CMF model is often assumed when inferring crustal magmatic processes from geological data. For instance, the periodic loss of grain–grain contiguity during heating has been used to explain the episodicity of deformation, metamorphism, and granitoid magmatism in low-pressure, high-temperature metamorphic terranes [10]. Tectonic surges, or the rapid displacement of high-grade crustal blocks, have been ascribed to weakening of the crust where the regional melt fraction exceeds the CMF [11]. The CMF model has been used to explain why basaltic magmas preferentially enter fissures as dikes and why rhyolites are most often represented by ash flows rather than lavas [12]. The agmatic and schlieric structures in migmatites, localized magmatic shear zones, the contact relationships between

granitoid intrusive suites, and the phenocryst content in lava flows and dikes have all been attributed to the loss of solid contiguity at the CMF [2,13,14].

A rheological model consistent with the experimental work of Rushmer [6] and Rutter and Neumann [7] would include a wider melt-fraction interval than assumed in the CMF model. However, the degree to which a more gradual rheological transition may influence interpretations of crustal magmatic processes is unknown. Crustal melting is one process in which the progress of melting and rate of heat transfer has been ascribed to the rheological transition between a partially molten solid and a viscous suspension [15–17]. We have conducted a series of transient numerical simulations of crustal melting in which we quantify the impact of the alternative rheological model on convective heat transfer and melting progress. Our results indicate that the form of the rheological transition may be one of the dominant controls on the dynamics of heat and mass transport during crustal anatexis.

2. Continuum model

We have adopted a two-phase continuum–mixture formulation to model crustal melting. This approach permits constitutive equations to be included in the governing equations which model the mechanical behavior of the mixture with increasing melt fraction. A comprehensive discussion of the continuum equations for double-diffusive heat and mass transfer in phase-change systems is available [18–22]. The variable viscosity form of the mixture continuum–conservation equations for phase change and convection in two dimensions are:

$$\frac{\partial v_j}{\partial x_j} = 0 \tag{1}$$

$$\frac{\partial}{\partial t}(\rho v_i) + \frac{\partial}{\partial x_j}(\rho v_j v_i) = -\frac{\partial p}{\partial x_i} + \frac{\partial}{\partial x_j}\left(\mu \frac{\partial v_i}{\partial x_j}\right) + \frac{\rho}{\rho^\ell}\frac{\partial v_i}{\partial x_j}\frac{\partial \mu}{\partial x_j} + g^\ell \gamma_o^\ell g_i \times \left[\beta_T^\ell (T - T_o) + \beta_C^\ell (C^\ell - C_o^\ell)\right] + \frac{\mu^\ell}{K_i}(f^\ell v_i^\ell) \tag{2}$$

$$\frac{\partial}{\partial t}(\rho T) + \frac{\partial}{\partial x_i}(\rho v_i T) = \frac{\partial}{\partial x_i}\left(\frac{k}{c_p^\ell}\frac{\partial T}{\partial x_i}\right) - \rho \frac{L}{c_p^\ell}\frac{\partial f^\ell}{\partial t} + \rho \frac{(c_p^\ell - c_p^s)}{c_p^\ell}\frac{\partial}{\partial t}(f^\ell T) \tag{3}$$

$$\frac{\partial}{\partial t}(\rho C) + \frac{\partial}{\partial x_i}(\rho v_i C) = \frac{\partial}{\partial x_i}\left(\rho f^\ell D^\ell \frac{\partial C}{\partial x_i}\right) + \frac{\partial}{\partial x_i}\left[\rho f^\ell D^\ell \frac{\partial}{\partial x_i}(C^\ell - C)\right] - \frac{\partial}{\partial x_i}[\rho v_i (C^\ell - C)] \tag{4}$$

The nomenclature for the formulae are presented in Table 1.

The continuum-mixture governing equations (Eqs. 1–4) require thermodynamic functions that link the enthalpy and composition to the local melt fraction. A pseudo-binary was projected from the 10 kbar NKM (Na_2O·Al_2O_3–K_2O·Al_2O_3–MgO+FeO) silica-, alumina-, and titania-saturated pseudo-ternary to generate this data. A discussion of the theory, limitations, and assumptions of this projection is presented elsewhere [18,23].

The rheology of the mixture is implemented by source terms that account for the different flow regimes as a function of the local melt fraction. For example, the last term on the right-hand side of the momentum conservation expression (Eq. 2) is the Darcy drag source term [19]. This relationship accounts for viscous drag between the solid and the interstitial melt as a function of the permeability, and provides the dominant balance between buoyancy and pressure when the melt fraction is low. According to the CMF model, with increasing melt fraction the solid grains lose contiguity over a small melt-fraction interval and form a viscous suspension with the melt. In our new physical model, the Darcy source imparts a drag on the mixture over a wider melt-fraction interval. In this way, we account for the additional drag resulting from the local variability in flow regimes within the melt-fraction interval over which the mechanical transition for the mixture occurs.

The dynamic viscosity of the suspension must include the contribution of the crystals, as well as the variable temperature and composition of the melt. Following Oldenburg and Spera [28], the permeabil-

Table 1
Key to the nomenclature in use for this study

Symbol	Description	Unit
c_p^a	heat capacity at constant pressure of constituent a	J/kg·K
C	solute concentration in the mixture	
C^a	solute concentration in constituent a	–[a]
D^a	diffusion coefficient of constituent a	m^2/s
f^a	mass fraction of constituent a	–[a]
g^a	volume fraction of constituent a	–[a]
g_i	component of gravitational acceleration	m/s^2
k	thermal conductivity	J/s·m·K
K_i	ith component of anisoptropic permeability	m^2
L	specific latent heat	J/K
p	static pressure or isotropic stress of the mixture	Pa
t	time	s
T	temperature	°C
v_i^a	ith component of mixture velocity of constituent a	m/s
β_C^a	coefficient of solutal expansion of constituent a	1/K
β_T^a	coefficient of thermal expansion of constituent a	1/K
E	melting efficiency	–[a]
ϑ	heat flux ratio	–[a]
γ^a	mass of constituent a per unit volume of constituent a	kg/m^3
Γ	permeability switching function	–[a]
κ	thermal diffusivity	m^2/s
Φ	viscosity switching function	–[a]
ρ	mass of mixture per unit volume of the mixture	kg/m^3
ρ^a	mass of constituent a per unit volume of the mixture	kg/m^3
μ	dynamic viscosity of mixture	Pa·s
μ^a	dynamic viscosity of constituent a	Pa·s
ν	kinematic viscosity of mixture	Pa·s
ν^a	kinematic viscosity of constituent a	Pa·s
Subscript		
o	reference value	
Superscript		
ℓ	liquid phase	
s	solid phase	

[a] Dimensionless.

ity and dynamic viscosity relationships are:

$$K = \Gamma K_o \left[\frac{(f^\ell)^3}{(1 - f^\ell)^2} \right] \tag{5}$$

$$\Gamma = \left\{ 0.5 + \frac{1}{\pi} \arctan\left[100 (f^\ell_{crit} = f^\ell) \right] \right\}^{-\xi} \tag{6}$$

$$\mu(T, C, f^\ell) = \left[1 - \Phi \left(\frac{1 - f^\ell}{f^\ell_{crit}} \right) \right]^{-2} \mu^\ell(T, C) \tag{7}$$

$$\Phi = 0.5 - \frac{1}{\pi} \arctan\left[100 \left(f^\ell_{crit} - f^\ell \right) \right] \tag{8}$$

We assume that, at low melt fraction, the permeability is related to the local melt fraction by the Blake–Kozeny–Carman equation (Eq. 5) [24]. K_o is a constant dependent on the multiphase region morphology [25]. This relationship is considered generally valid in the laminar flow regime and for melt-volume fractions less than 0.5 [26]. At high melt fraction, the dynamic viscosity of the melt is calculated using the Shaw model [27] and the drag from suspended crystals is modeled by the Krieger–Dougherty relation [40] (Eq. 7) as presented in Wildemuth and Williams [5].

Following Oldenburg and Spera [28], mechanical

differences between the solid and melt are implemented by arctangent switching functions (Eqs. 6 and 8) multiplied to the relevant terms in the governing equations [28]. Both the permeability and the dynamic viscosity are switched in this manner. These switching functions ensure that the Darcy drag source is included when the local melt fraction (f^ℓ) is low and the viscosity contribution of suspensions is included for $f^\ell \geq 0.5$. We initiate the transition between crystal-supported and fully fluid behavior at $f^\ell = 0.5$ in all simulations as this value may be important in magmatic systems [13,29]. The melt-fraction interval over which the rheological transition takes place is determined by the permeability switching-function power law (ζ in Eq. 6). We do not smooth the viscosity switching function, as a more gradual transition to a viscous suspension would increase the local mixture viscosity at a given melt fraction. Therefore, our results are an upper end-member for convective heat transfer with respect to the mixture viscosity. The remaining source terms accounting for the energy of phase change are discussed elsewhere [18,19,30].

We consider six values of ζ which span a range of possible gradations of the rheological transition. At one limit is the traditional CMF model that requires the Darcy drag source vanish over a small increase in melt fraction between 28 and 50% melt. The CMF model is implemented in the $\zeta = 10$ simulations where the Darcy drag source approaches zero between $0.5 < f^\ell < 0.57$. More abrupt rheological transitions ($\zeta > 10$) were tested, but did not produce appreciably different results than the $\zeta = 10$ simulations. The rheological transition occurs over a wider melt-fraction interval for smaller values of ζ. The permeability and kinematic viscosity ($= \mu/\rho$), modified by the switching functions with the various power laws, are illustrated in Fig. 3. The shapes of the viscosity profiles in Fig. 3 are discussed in detail elsewhere [23].

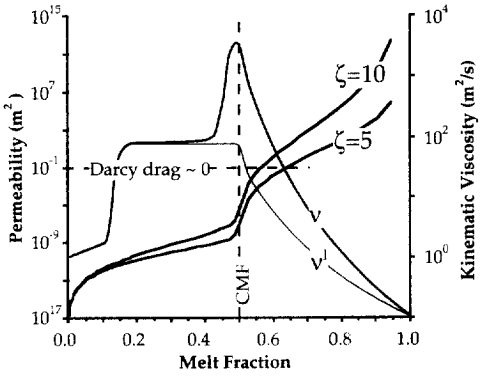

Fig. 3. Plot of the kinematic viscosity and permeability against melt fraction (f^ℓ). The two viscosity curves represent the viscosity of the melt (ν^ℓ) and the effective viscosity of the melt + crystal mixture (ν). ν^ℓ and f^ℓ are both functions of temperature, whereas ν is a function of both temperature and f^ℓ. The two permeability curves represent the CMF model ($\zeta = 10$) and the most gradual rheological transition considered ($\zeta = 5$). The four other rheological transition models are bounded by these limits. Viscous drag imposed on the interstitial melt approaches zero where the permeability curves intersect the Darcy drag ~0 line.

3. Model assumptions

We assume that the source region remains undrained through the duration of the simulations (160 yr). Also, our implementation of the mixture model does not allow us to consider diapiric instabilities of the growing melt layer into the unmelted roof. Newhouse and Pozrikidis [31] have carried out a linear stability analysis of the growth rate of diapiric instabilities. The amount of time before the amplitude of the diapiric instabilities doubles is approximately an order of magnitude longer than the duration of the simulations. Therefore, diapiric instabilities are unlikely to be significant on the time scales considered in the simulations.

The mixture model does not allow for relative motion between phases in the viscous flow regime, so processes such as crystal settling are not considered. This assumption does not limit the utility of the mixture model if the particle motion is dominated by the flow field of the carrier fluid. This is likely to be the case as long as typical velocities of the crystal–melt mixture exceed the predicted Stokes settling velocities of the dispersed crystals. Assuming the particle Reynolds number is less than one, the settling velocity of crystals can be obtained by equating the Stokes drag formula to the gravitational buoyancy force [32]. Stokes settling velocities calculated for 1–10 cm crystals are less than typical average velocities of the crystal–melt mixture in the viscous flow regime. Therefore, differential motion between the crystals

and melt is unlikely to significantly influence the flow of the mixture.

In the development of the governing equations (Eqs. 1–4) we assume: (1) the velocity of the solid phase is zero ($v_s = 0$); (2) the mixture is fully saturated ($g^\ell + g^s = 1$); (3) the flow of the melt is laminar and Newtonian; (4) the Boussinesq approximation is valid; (5) local thermodynamic equilibrium is ($T^\ell = T^s = T$) maintained; (6) the phase specific heats are constant, though not necessarily equal; (7) the diffusion of species in the solid phase is negligible; (8) the solid phase is rigid and free of internal stresses; and (9) the permeability of the partially molten solid is isotropic [37]. The assumption of mixture saturation and a stress-free solid also implies that the phase densities and thus the phase volume and mass fractions are equal ($\rho^s = \rho^\ell$, $f^i = g^i$).

4. Model description and geological motivation

We defined a model protolith with a non-linear relationship between temperature and melt fraction (melt productivity) based on the metapelite used in the experiments of Vielzeuf and Holloway [33]. Dehydration melting of biotite in this rock composition may produce up to ~55% melt over a small temperature interval near 850°C, thereby exceeding the CMF. This lithology thus provides a useful mechanical end-member for our calculations, as the CMF is exceeded at lower temperatures than for many crustal rocks [34]. The phase relations were experimentally derived by Patiño Douce and Johnston [38] using their own data along with those of Vielzeuf and Holloway [33] and Le Breton and Thompson [39]. The model equilibrium melt productivity curve is compared to the experimental data in Fig. 4.

The model dimensions and boundary conditions are based on conditions expected in the vicinity of a 200-m-wide basaltic sill in the mid-to-lower continental crust (underplating) [23]. The 200 × 200 m computational domain was represented by a 70 × 70 node, variable-spaced grid, refined in both dimensions toward the heated boundary (Fig. 5). The solutions are assumed to be symmetric around the right margin of the computational domain. A grid refinement study was undertaken to ensure that the simulations were independent of the spatial and temporal

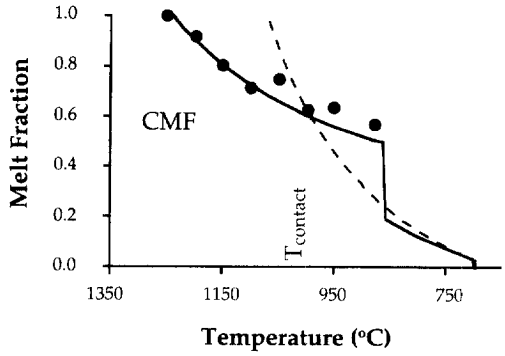

Fig. 4. Plot of the relationship between temperature and melt fraction (melt productivity) for the two lithologies considered in the study. The solid line illustrates the melt productivity of the model metapelite based on the composition considered by Vielzeuf and Holloway [33]. The dashed line is the hypothetical crustal composition with a more linear melt productivity. The circles are the experimental data of Vielzeuf and Holloway [33]. The melt productivity of the hypothetical crustal composition was constructed so that both systems had the same melt fraction at the contact temperature ($T_{contact}$).

grid discretization. Particular attention was paid to the grid dependence at the initiation of convection. Heat flux over the first 2 years of the CMF model simulations ($\zeta = 10$) varied less than 1% after increasing the density of the vertical distribution of grid points by a factor of four.

At the start of the simulations, the temperature of the country rock was uniform with a value of

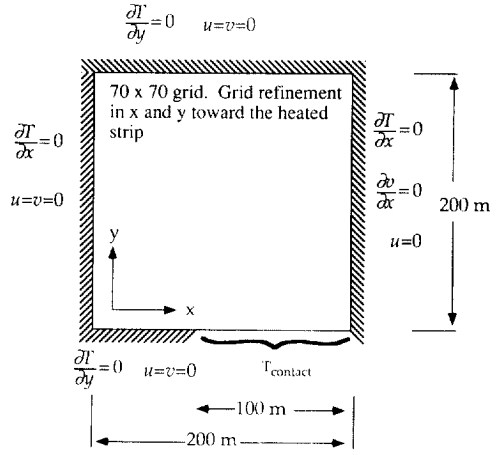

Fig. 5. Schematic of the computational domain. We used a 70 × 70 node grid with a refinement factor of 1.6 in x and 1.4 in y.

Table 2
Values for the various material properties and for the initial and boundary conditions used in the numerical simulations

Thermophysical and rheological properties	
Specific heat (J/kg·K)	1.04×10^3
Thermal conductivity (W/m·K)	1.9
Density (kg/m^3)	2.507×10^3
Kinematic viscosity (m^2/s)	see text
Schmidt number (ν^ℓ / D)	1.0×10^6
Latent heat (J/kg)	1.0×10^5
Permeability coefficient (m^2)	5.56×10^{-10}
Thermal expansion coefficient (K^{-1})	1.05×10^{-4}
Solutal expansion coefficient	1.55×10^{-1}
Critical melt fraction	0.5
Initial and boundary conditions	
Pelite starting composition	0.325
Initial temperature (°C)	600.0
Contact temperature (°C)	1000.0
Total time duration of simulations (s)	5×10^9

600°C. The roof and walls were thermally insulated. We implemented basaltic underplating by fixing the temperature along a 100-m strip from the center of the lower boundary to the right wall to 1000°C. Free-slip conditions were assigned to the right wall and no-slip conditions on the remaining boundaries. A summary of the various model parameters and boundary conditions used in the simulations is given in Table 2 and Fig. 5.

We based the numerical algorithm on the control-volume formulation [35] and used the PHOENICS algorithm [36] to solve Eqs. 1–4. The mass fractions were updated iteratively following the procedures outlined in Prakash and Voller [30]. Details of the numerical procedures and other aspects of this application of the PHOENICS algorithm are provided elsewhere [18,23,30].

5. Results and discussion

In previous studies, we demonstrated the sensitivity of convective heat transport on the melt productivity (increase in melt fraction with temperature) of the protolith, viscosity of the melt, and the melt fraction at which the rheological transition takes place (CMF) [18,23]. In the ensuing sections, we demonstrate the influence on convective heat transfer of the rheological transition between a partially molten solid and a viscous suspension. Five sets of simulations were performed, using the same values for the CMF and K_o but with differing values of ζ. The CMF model is approximated in the simulations in which $\zeta = 10$, where the rheological transition occurred over the smallest melt-fraction interval.

5.1. Initiation of convection

In all of the simulations, convection initiated with buoyant instabilities along the contact adjacent to the right margin of the computational domain. As convection developed, the instabilities propagated toward the left edge of the heated strip. The initial separation between the upwellings was approximately 20–25 m. Upward propagation of the melting front led to merging of the buoyant crystal–melt plumes. In all cases, when the cavity aspect ratio was approximately 1 : 1, convection was dominated by a single counterclockwise-rotating convection cell. This evolution in the style of convection proceeded most rapidly in the $\zeta = 10$ simulations.

We defined the initiation of convection to be when the heat flux across the heated strip was elevated by 1% relative to conduction. In the $\zeta = 10$ simulations (our closest approximation for the CMF model), convection began approximately 0.8 years after initiation when the boundary enclosing the region which exceeded the CMF had propagated 1.1 m from the contact. This is somewhat further than would be predicted based on buoyant thermal instabilities alone. The critical Rayleigh number (Ra_{crit}) for the onset of thermal convection in a fluid heated from below is approximately 1000 or 2000 [32]. We assume a Ra_{crit} of 2000 and invert the Rayleigh number to obtain the theoretical thickness of the melt lens at the onset of convection:

$$h = 3\sqrt{\frac{\mu\kappa Ra_{crit}}{\rho^o g\alpha\Delta T}} \tag{9}$$

Using typical values obtained in the simulations, we calculate the theoretical thickness of the melt lens prior to convection to be between 0.3 and 0.7 m. We have found that, for the pelite system during underplating, double-diffusive effects can delay the onset of convection and impede convective vigor [18]. Therefore, theoretical estimates based on thermal buoyancy alone may underestimate the time to

the onset of convection and overestimate convective vigor during the anatexis of some crustal rocks.

We found the time duration prior to the initiation of convection was sensitive to the melt-fraction interval for the rheological transition in addition to double-diffusive effects. More gradual transitions ($\zeta < 10$) increased the amount of time and the minimum height of the melt lens before convection began. For instance, 160 years after initiation of the simulation with the most gradual rheological transition ($\zeta = 5$), the boundary enclosing the region exceeding the CMF had propagated approximately 35 m from the simulated contact with the sill. Although this is over 100 times more distant than would be predicted by Eq. 9 for convection to begin by thermal buoyancy alone, the temperature profile in the crustal rocks was conductive. Our results indicate that classical dimensionless analysis and numerical simulations that assume an abrupt rheological transition may significantly underestimate the time required before the onset of convection.

5.2. *Influence of rheological transitions on the progress of melting*

Fig. 6 depicts the thermal state of the system, after 79.3 years, for simulations using three different rheological models. Viscous flow of the crystal–melt mixture, indicated by the velocity vectors, is enclosed within the region which exceeds the CMF ($f^{\ell} = 0.5$). The CMF is approximately coincident with the biotite dehydration-melting isopleth. The distance above the heated strip that the isopleth propagated as a function of time is illustrated in Fig. 7 for the three simulations. Along the right wall of the computational domain, the height was 137 m after 79.3 years for the $\zeta = 10$ simulations. For $\zeta = 8$ and $\zeta = 6$ the isopleth had propagated 120 m and 61 m respectively. The distance between the predicted positions increased as a function of time. Therefore, the relationship between convective heat transfer and the melt-fraction interval for the rheological transition can change the predicted positions of isotherms by up to a factor of two.

Fig. 8 depicts the efficiency of melt generation (E) as a function of time for the five series of simulations. $E = 2.0$ indicates that twice as much melt was generated as was predicted to have been produced at

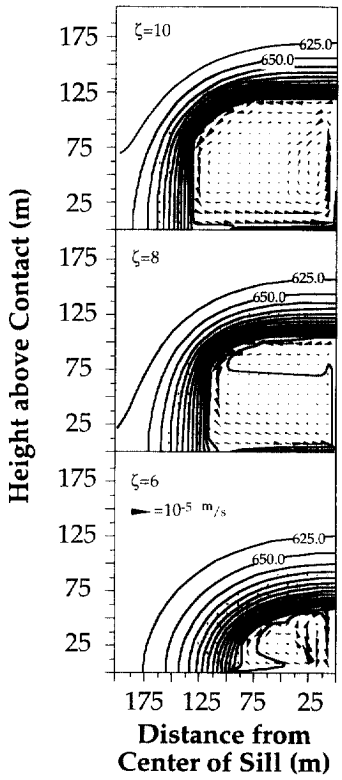

Fig. 6. Sample results 79.3 years after the initiation of the simulations with $\zeta = 10$, 8, and 6. Contours are of temperature in °C. Viscous flow, indicated by the velocity vectors, is enclosed by the region exceeding the CMF ($f^{\ell} = 0.5$). Typical melt velocities in the porous flow regime are 6–8 orders of magnitude less than viscous flow velocities in the mixture.

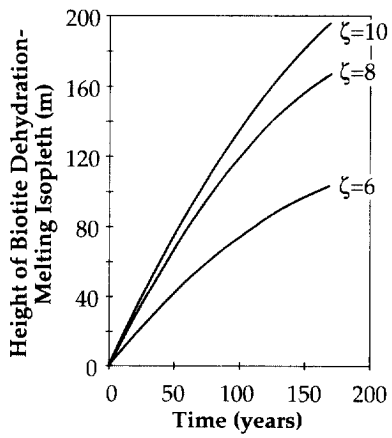

Fig. 7. Distance the biotite dehydration isopleth had propagated as a function of time, for simulations with $\zeta = 10$, 8, and 6.

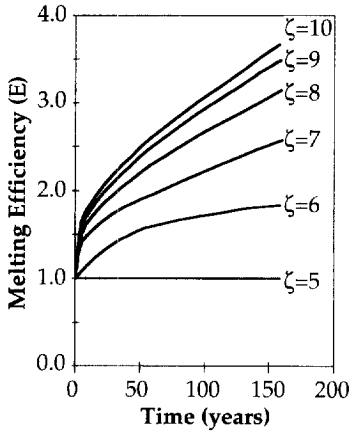

Fig. 8. Melting efficiency (E) as a function of time predicted by the simulations with the various rheological models. We define E as the mass of melt generated in the simulations relative to the mass of melt predicted to be generated in the absence of convection.

the same time by conduction alone. After 95 years, E was approximately 3.0 in the $\zeta = 10$ simulations. The simulations using $\zeta = 5$, however, at no time produced more melt than would be predicted by conduction alone. We conclude that predictions of melting progress in high-grade igneous and metamorphic terranes may vary significantly within the range of the uncertainty in the rheological transition between solid and melt.

5.3. Sensitivity of thermal evolution to rheological transitions

Fig. 9 depicts the change of the thermal flux ratio (ϑ) as a function of time for the various values of ζ. We define ϑ as the ratio of the average heat flux across the heated strip measured in a convection simulation relative to conduction. The flux ratio is thus analogous to the Nusselt number which is often used to characterize the efficiency of convection for steady-state convective heat transport. For example, $\vartheta = 2.0$ indicates that the heat flux is twice that of conduction. Convective heat flux did not monotonically increase, which resulted in some scatter in ϑ. This observation is consistent with other experiments and simulations, where such irregularities have been attributed to the time-dependent nature of the solidus front growth rate [37]. Accordingly, the curves in Fig. 9 are a best fit to the computed flux ratio.

After 79.3 years, $\vartheta = 5.6$, 4.6, and 2.0 for the simulations with $\zeta = 10$, 8, and 6, respectively. The $\zeta = 8$ and $\zeta = 6$ simulations resulted in a 17 and 65% reduction, respectively, in the efficiency of convective heat transfer relative to the $\zeta = 10$ simulation. The flux ratio continuously diverged as a function of time. However, the largest change in ϑ occurred for $\zeta = 5$, 6, and 7. For instance, after approximately 143 years, ϑ was 7.35 and 7.13 in the $\zeta = 10$ and $\zeta = 9$ simulations, respectively. Thus, a factor of one decrease in ζ caused a 4.3% reduction in the efficiency of heat transfer. However, decreasing ζ from 8 to 7 resulted in a 33% reduction in heat transfer. Therefore, ϑ was more sensitive to changes in ζ in systems with a more gradual rheological transition.

5.4. Relative importance of melt productivity and the rheological transition

In another study, we evaluated changes in the heat transfer and progress of melting as a function of the melt productivity of the protolith (increase in melt fraction with temperature) [18]. We compared the convective heat transfer during anatexis of two protolith compositions: (1) the pelitic composition adopted in this study with a non-linear increase in f^l with temperature; and (2) a hypothetical composition

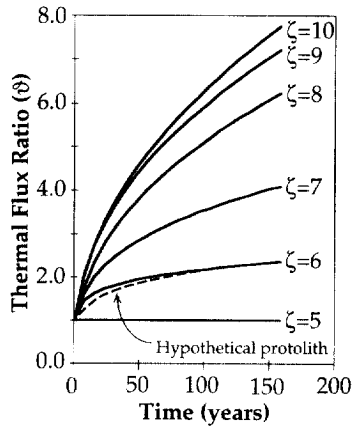

Fig. 9. Heat flux ratio (ϑ) as a function of time predicted by the simulations with the various rheological models. We define ϑ as the heat flux across the heated strip calculated during the simulations relative to that predicted in the absence of convection. The dashed line indicates ϑ for the hypothetical composition with the linear melt productivity and $\zeta = 10$.

with a linear melt productivity. The melt productivity curves for the two lithologies are compared in Fig. 4. The melt productivity of many crustal rocks fall between these extremes [34]. The two compositions thus represent end-members for a continuum of possible melt productivities from crustal rocks. The various boundary and initial conditions of the simulations were identical to those of this study.

Fig. 9 depicts ϑ as a function of time for the hypothetical composition with linear melt productivity and $\zeta = 10$. This figure illustrates that convective heat transfer may be significantly suppressed during melting of less fertile protoliths. For example, after 79.3 years $\vartheta = 2.0$ for the hypothetical protolith with the linear melt productivity. For the model pelite at the same time, ϑ was 280% larger. However, the variability in ϑ resulting from the tested rheological transitions exceeds the predicted variability as a function of protolith composition. Adopting $\zeta = 5$ for the model protolith composition, for example, suppressed convection to the extent that the calculated heat flux was equivalent to conduction through the duration of the simulations. We conclude that, for a wide range of fertile crustal rocks, the rheological transition between solid and melt may be one of the dominant factors controlling convective vigor in crustal magmatic systems.

6. Conclusions

The results of low-melt fraction deformation experiments indicate that the rheological transition between crystal-supported to fully fluid behavior may be more gradual than stipulated by the CMF model. However, it is uncertain what impact this may have on interpretations of geologic processes that appeal to the loss of contiguity at the CMF.

The hybrid model of Oldenburg and Spera [28] may be easily adapted to accommodate a more gradual rheological transition. Using the modified Oldenburg and Spera [28] model, we conducted numerical simulations to evaluate the relationship between crustal anatexis, convective heat transfer, and the rheological transition. A more gradual rheological transition may significantly delay the initiation of convection. An insignificant amount of convective heat transfer was observed in the $\zeta = 5$ simulations, even though the boundary enclosing the region which exceeded 50% melt had propagated 34.7 m from the contact. Heat flux was between one ($\vartheta = 1.0$) and eight times ($\vartheta = 8.0$) that of conduction alone, depending on the selection of rheological models.

Both the rheological transition and the lithology of the protolith contribute to convective heat flux. Two protolith compositions were analyzed which bracket the melt productivity of a wide range of common crustal rocks. We found that convective heat transfer and melting were more strongly influenced by the selection of rheological transition model than by the melt productivity of the protolith. We conclude that the mechanical behavior of high-melt-fraction igneous and metamorphic systems may be a dominant factor influencing the generation of felsic melts.

Acknowledgements

We gratefully acknowledge the editorial comments from Dr. Georges Ceuleneer, Dr. Frank Spera, and an anonymous reviewer. Partial funding for this work was provided by NSF Grant 9508291. *[AC]*

References

[1] A.A. Arzi, Critical phenomena in the rheology of partially melted rocks, Tectonophysics 44 (1978) 173–184.
[2] I. van der Molen, M.S. Paterson, Experimental deformation of partially-melted granite, Contrib. Mineral. Petrol. 70 (1979) 299–318.
[3] R. Roscoe, The viscosity of suspensions of rigid spheres, Br. J. Appl. Phys. 3 (1952) 267–269.
[4] D.J. Jeffrey, A. Acrivos, The rheological properties of suspensions of rigid particles, J. Am. Inst. Chem. Eng. 22 (1976) 417–432.
[5] C.R. Wildemuth, M.C. Williams, Viscosity of suspensions modeled with a shear-dependent maximum packing fraction, Rheol. Acta 23 (1984) 627–635.
[6] T. Rushmer, An experimental deformation study of partially molten amphibolite: application to low-melt fraction segregation, J. Geophys. Res. 100 (1995) 15681–15695.
[7] E.H. Rutter, D.H.K. Neumann, Experimental deformation of partially molten Westerly granite under fluid-absent conditions, with implications for the extraction of granitic magmas, J. Geophys. Res. 100 (1995) 15697–15715.
[8] J.L. Vigneresse, B. Pierre, C. Michel, Rheological transitions during partial melting and crystallization with appli-

cation to felsic magma segregation and transfer. J. Petrol. 37 (1996) 1579–1600.
[9] E.W. Sawyer, personal communication, 1997.
[10] K. Stüwe, M. Sandiford, R. Powell, Episodic metamorphism and deformation in low-pressure high-temperature terranes, Geology 21 (1993) 829–832.
[11] L.S. Hollister, M.L. Crawford, Melt-enhanced deformation: a major tectonic process, Geology 14 (1986) 558–561.
[12] W.S. Pitcher, The Nature and Origin of Granite, Blackie, London, 1993, 321 pp.
[13] B.D. Marsh, On the crystallinity, probability of occurrence, and rheology of lava and magma, Contrib. Mineral. Petrol. 78 (1981) 85–98.
[14] S.M. Wickham, The segregation and emplacement of granitic magmas, J. Geol. Soc. Lond. 144 (1987) 281–297.
[15] D. Bittner, H. Schmeling, Numerical modeling of melting processes and induced diapirism in the lower crust, Geophys. J. Int. 123 (1995) 59–70.
[16] A.R. Cruden, H. Koyi, H. Schmeling, Diapiric basal entrainment of mafic into felsic magma, Earth Planet. Sci. Lett. 131 (1995) 321–340.
[17] F. Raia, F.J. Spera, Simulations of crustal anatexis: implications for the growth and differentiation of the continental crust, submitted to J. Geophys. Res.
[18] S.A. Barboza, G.W. Bergantz, Melt productivity and rheology: complementary influences on the progress of melting, Num. Heat Transfer 31 (1997) 375–392.
[19] W.D. Bennon, F.P. Incropera, A continuum model for momentum, heat and species transport in binary solid–liquid phase change systems. I. Model formulation, Int. J. Heat Mass Transfer 30 (10) (1987) 2161–2170.
[20] C. Beckermann, R. Viskanta, Natural convection solid/liquid phase change in porous media, Int. J. Heat Mass Transfer 31 (1) (1988) 35–46.
[21] J. Ni, C. Beckermann, A volume-averaged two-phase model for transport phenomena during solidification, Metall. Trans. B 22B (1991) 349–361.
[22] C.M. Oldenburg, F.J. Spera, Numerical modeling of solidification and convection in a viscous pure binary eutectic system, Int. J. Heat Mass Transfer 34 (1991) 2107–2121.
[23] S.A. Barboza, G.W. Bergantz, Dynamic model of dehydration melting motivated by a natural analog: applications to the Ivrea–Verbano zone, northern Italy, Trans. R. Soc. Edinburgh 87 (1996) 23–31.
[24] V.R. Voller, C. Prakash, A fixed grid numerical modeling methodology for convection–diffusion mushy region phase-change problems, Int. J. Heat Mass Transfer 30 (8) (1987) 1709–1719.
[25] S. Asai, I. Muchi, Theoretical Analysis and Model Experiments on the Formation Mechanism of Channel-Type Segregation, Transactions: Iron and Steel Institute of Japan (ISIJ) 18, 1978, pp. 90–98.
[26] R.B. Bird, W.E. Stewart, E.N. Lightfoot, Transport Phenomena, Wiley, New York, 1960, 780 pp.
[27] H.R. Shaw, Viscosities of magmatic liquids: an empirical method of prediction, Am. J. Sci. 272 (1972) 870–893.
[28] C.M. Oldenburg, F.J. Spera, Hybrid model for solidification and convection, Num. Heat Transfer B 21 (1992) 217–229.
[29] C.F. Miller, E.B. Watson, T.M. Harrison, Perspectives on the source, segregation and transport of granitoid magmas, Trans. R. Soc. Edinburgh 79 (1988) 135–156.
[30] C. Prakash, V.R. Voller, On the numerical solution of continuum mixture model equations describing binary solid–liquid phase change, Num. Heat Transfer B 15 (1989) 171–189.
[31] L.A. Newhouse, C. Pozrikidis, The Rayleigh–Taylor instability of a viscous liquid layer resting on a plane wall, J. Fluid Mech. 217 (1990) 615–638.
[32] D.L. Turcotte, G. Schubert, Geodynamics: Applications of Continuum Physics to Geologic Problems, Wiley, New York, 1982, 450 pp.
[33] D. Vielzeuf, J.R. Holloway, Experimental determination of the fluid-absent melting relations in the pelitic system, Contrib. Mineral. Petrol. 98 (1988) 257–276.
[34] G.W. Bergantz, R. Dawes, Aspects of magma generation and ascent in continental lithosphere, in: M.P. Ryan (Ed.), Magmatic Systems, Academic, San Diego, 1994, pp. 291–317.
[35] S.V. Patankar, Numerical Heat Transfer and Fluid Flow, Hemisphere, New York, 1980, 197 pp.
[36] H.I. Rosten, D.B. Spalding, The PHOENICS Reference Manual, CHAM TR/200, 1987.
[37] W.D. Bennon, F.P. Incropera, A continuum model for momentum, heat and species transport in binary solid–liquid phase change systems. II. Application to solidification in a rectangular cavity, Int. J. Heat Mass Transfer 30 (10) (1987) 2171–2187.
[38] A.E. Patiño Douce, A.D. Johnston, Phase equilibria and melt productivity in the pelitic system: implications for the origin of peraluminous granitoids and aluminous granulites, Contrib. Mineral. Petrol. 99 (1990) 202–218.
[39] N. Le Breton, A.B. Thompson, Fluid-absent (dehydration) melting of biotite in metapelites in the early stages of crustal anatexis, Contrib. Mineral. Petrol. 99 (1988) 226–237.
[40] I.M Krieger and T.J. Dougherty, A mechanism for non-Newtonian flow in suspensions of rigid spheres, Trans. Soc. Rheol. 3, 137–152.